ChemPlusChem

A Multidisciplinary Journal Centering on Chemistry

Chemistry Europe

European Chemical Societies Publishing

Accepted Article

Title: Design, Synthesis and Antitumor Activity Evaluation of Novel Cyclometalated 2H-Indazole Ru(II) and Ir(III) Complexes

Authors: Kaushik Chanda, Ramdas Nishanth Rao, Rajeeva Lochana Panchangam, Venkatraman Manickam, and Musuvathi Motilal Balamurali

To be cited as: *ChemPlusChem* 10.1002/cplu.202000516

Link to VoR: https://doi.org/10.1002/cplu.202000516

WILEY-VCH

Synthesis and Antitumor Activity Evaluation of Cyclometalated *2H*-Indazole Ruthenium(II) and Iridium(III) Complexes

Ramdas Nishanth Rao,[a] Rajeeva Lochana Panchangam,[b] Venkatraman Manickam,[b] Musuvathi Motilal Balamurali,*[c] and Kaushik Chanda*[a]

[a]*Ramdas Nishanth Rao,* [+] *Prof. Kaushik Chanda* Department of Chemistry, School of Advanced Science, Vellore Institute of Technology, Vellore-632014, India.

[b]*Rajeeva Lochana Panchangam,* [+] *Prof. Venkatraman Manickam* Department of Biosciences, School of Biosciences and Technology, Vellore Institute of Technology, Vellore-632014, India.

[c]*Prof. Musuvathi Motilal Balamurali* Chemistry Division, School of Advanced Sciences, Vellore Institute of Technology, Chennai Campus, Chennai-600127, India

[+]These authors contributed equally to this work.

Email: chandakaushik1@gmail.com

mmbala@gmail.com

Abstract: In this work, a series of novel C-N cyclometalated 2*H*-indazole Ru(II) and Ir(III) complexes were synthesized wherein chelating ligands with substituents like H, and isopropyl group in the R_4 position of the phenyl ring of 2*H*-indazole chelating ligand are present. The cytotoxicity of Ru(II) and Ir(III) complexes has been evaluated against different human cancer cell lines (HeLa, MCF-7, and A549) in a concentration-dependent manner. The new iridium complex with isopropyl substituent in the phenyl ring of 2*H*-indazole moiety showed good cytotoxic activity against MCF-7 cells with IC_{50} value 3.5 µM. The complex also exhibited cytotoxicity comparable to that of cisplatin. The ability of this compound inducing apoptosis was tested by nuclear condensation, cell membrane blebbing and caspase 3/7 activation. Further, this novel iridium complex is capable of inhibiting cancer cell migration when tested in MCF-7 cell line. Subsequently, we have studied the DNA binding and protein binding ability of the newly synthesized iridium complex.

10.1002/cplu.202000516

Graphical Abstract

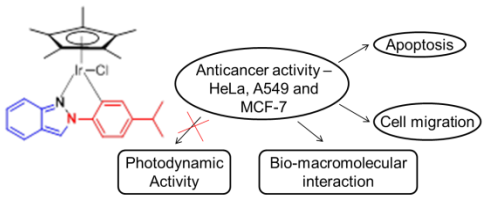

Introduction

The role of metal complexes in biological[1-3] and medical sciences[4,5] has been well established for the past several decades. With the emergence of metallo-therapeutics several achievements were made in the field of medical research.[6,7] Interestingly, in the past two decades therapeutic stimuli-responsive (pH, enzyme, light, temperature, etc) metallo-drugs were reported.[8,9] Despite the advancements in drug research and understanding of the complex nature, cancer still remains as the major cause of death in human population. Though the serendipitous discovery of cisplatin and platinum containing drugs like carboplatin, and oxaliplatin lead to the development of varieties of elemental anticancer drugs,[10] they lack the much needed target specificity.[11] Novel approaches towards enhancing the efficacy of therapeutic treatments are being continuously developed. Recent research outcomes on metal complexes have provided the unique ability to alter pharmacology, efficacy and reduced side effects as cancer drugs. New therapeutic strategies with these metal complexes lead to the bottom up approach for the rational design of novel anticancer agents which can enhance the efficacy and tolerability. In tandem with several platinum based metallodrugs, significant efforts have been dedicated to develop Ru, Ir, Os, Re, and Rh based metallodrugs.[12] Several reports have shown that the *in vivo* antimetastatic activity of ruthenium complexes[13] have paved way for the development of more nontoxic ruthenium(II) and iridium(III) complexes as angiogenesis inhibitors.[14] The anticancer activity can be modulated uniquely through structural modifications in ligands around the metal center and has been confirmed through the recently developed Pt and Ru anticancer compounds. Very good anticancer activity was observed with the rationally designed cyclometalated Ru(II) and Ir(III) complexes against several cancer cell lines.[15] Recently, with the emergence of synthesised small drug-like heterocyclic molecules and their use as potential chelating ligands for the

synthesis of metal complexes is well recognized as a tool for the generation of promising metallodrugs with substantial anticancer property. The design concept of the currently synthesized complexes has originated from the recognition of the biological role of core 2*H*-indazole moiety having antitumor,[16] HIV-protease inhibition,[17] anti-inflammatory,[18] and modulatory role on estrogen receptors.[19] Interestingly, the 2*H*-indazole moiety ligands possess the ability to target the drug resistant, epidermal growth factor receptor (EGFR) over expressing tumors, and are found in many best selling drugs such as pazopanib, and niraparib.[20] Moreover, 2*H*-indazole ligands also owe photo-physical property which makes them a promising candidate with inherent potential for theranostic applications.[21] Further, there are several reports in the literature on the application of Ru (II)[22] and Ir (III)[23] complexes in photodynamic therapies for the treatment of cancer or certain types of infections. In addition, the core 2*H*-indazole can be easily modified for the synthesis of diversely fused heterocycles with significant intellectual appeals.

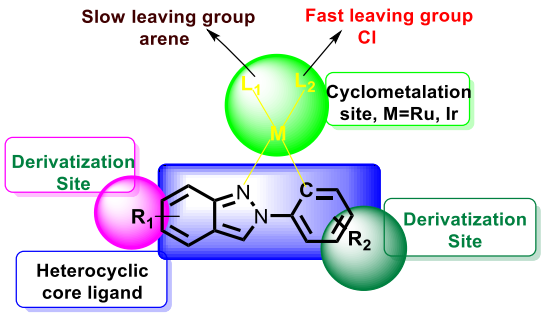

Figure 1. The design of Novel Cyclometalated Indazole Ru(II) and Ir(III) Complexes

The figure 1 shows the readily available C-N site in indazole moiety for cyclometalation to construct organometallic complexes. Gratifyingly, the easy derivatization of the phenyl ring on both sides of the C-N functionality can be achieved for the structure activity relationship (SAR). In continuation of our research to develop newer synthetic methodologies for the construction of

heterocycles and subsequent bioactivity evaluation,[24] we propose to synthesize an array of organometallic ruthenium and iridium complexes having 2*H*-indazole as major backbone. With the aim of increasing the available lead metallo-drugs having cost-effective, wide spectrum anti-cancer therapeutic roles, we believe that organometallic complexes with these polyvalent ligands are completely innovative in the bibliography, and the observed results from anticancer studies leaves a new footprint for designing metal drugs with diverse functions.

Results and Discussion

At the onset of our study, the synthesis of substituted 2*H*-indazole **3** ligand which could be achieved by the simultaneous formation of C-N, and N-N bonds through the one-pot synthetic transformation. The synthetic methodology was initiated by the Cu_2O rhombic dodecahedra catalyzed cyclization reaction between 2-bromobenzaldehyde **1**, NaN_3 and aromatic amine **2** and 1,10-phenanthroline as ligand in DMSO solvent to obtain substituted 2*H*-indazole **3** derivatives as shown in Scheme 1.[24c]

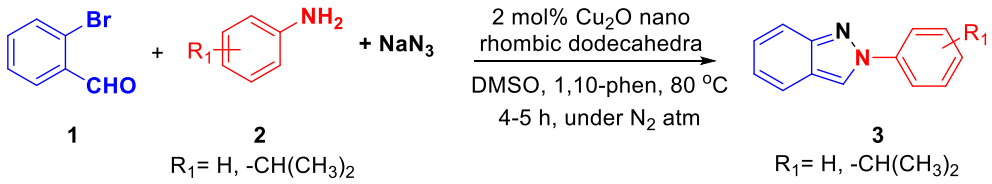

Scheme 1. Cu(I) catalyzed synthesis of key 2*H*-indazole ligands.

The synthesized ligands **3** were characterized by ^1H, ^{13}C NMR, Mass and IR spectroscopy. With the key ligands in our hands, we attempted to synthesize the organometallic complexes with ruthenium and iridium metals. The synthesis of ruthenium and iridium cyclometalated complexes using $[RuCl_2(\eta^6\text{-}p\text{-cymene})]_2$ and $[(\eta^5\text{-}C_5Me_5)IrCl_2]_2$ with key 2*H*-indazole ligands **3** is shown in Scheme 2. The synthesis of ruthenium cyclometalated complexes **4a-b** was achieved by treating

10.1002/cplu.202000516

ligands **3a-b** with $[RuCl_2(\eta^6\text{-}p\text{-cymene})]_2$ and sodium acetate in dichloromethane at room temperature for 20 h in 72-75% yield in Scheme 2.

Scheme 2. Synthesis of 2*H*-indazole contained cyclometalated Ru(II) and Ir(III) complexes.

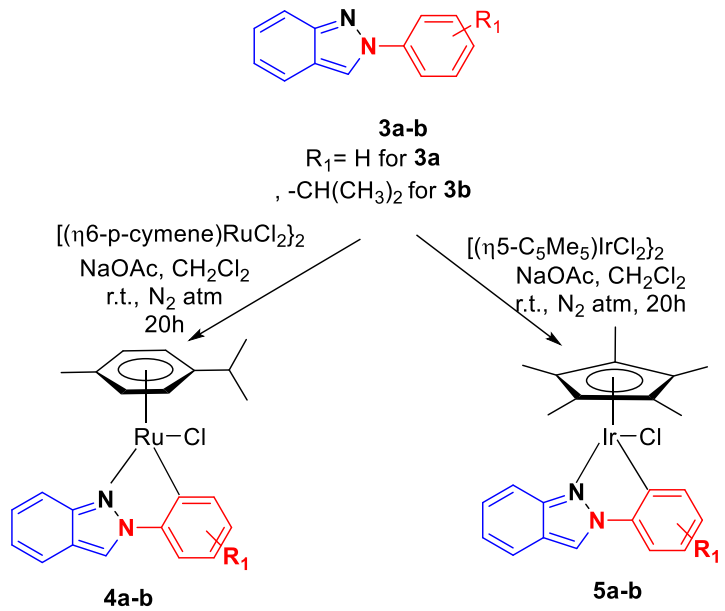

Similarly, half sandwich iridium(III) complexes **5a-b** were obtained from $[(\eta^5\text{-}C_5Me_5)IrCl_2]_2$ using similar synthetic conditions for 20 h in 82-85% yields. Accordingly, the table 1 demonstrated the series of complexes with yields. The structures of all complexes were unequivocally confirmed by ^1H, ^{13}C NMR and ESI-MS while their high degree of purity was determined by HRMS analysis.

Table1. List of synthesized cyclometalated complexes of Ru(II) and Ir(III).

Complex	R1	Metal Complex	Yield
4a	-H	$[(\eta6\text{-}p\text{-cymene})RuCl_2]_2$	72 %
4b	$-CH(CH_3)_2$	$[(\eta6\text{-}p\text{-cymene})RuCl_2]_2$	75 %
5a	-H	$[(\eta5\text{-}C_5Me_5)IrCl_2]_2$	82 %
5b	$-CH(CH_3)_2$	$[(\eta5\text{-}C_5Me_5)IrCl_2]_2$	85 %

In the ^{1}H NMR spectra of **4a-b**, the disappearance of one aromatic proton and introduction of four doublets at 5.1-5.9 ppm, a singlet at 2.0-2.1 ppm, and two doublets at 0.6-0.8 ppm for six protons corresponding to *p*-cymene confirms the formation of 2*H*-indazole contained ruthenium complexes. Likewise, for half-sandwich iridium (III) complexes **5a-b,** ^{1}H NMR spectrum displayed a singlet at 1.7 ppm for fifteen protons corresponding to pentamethylcyclopentadienyl (C_5Me_5) moiety.

In order to evaluate any synthesized molecule as a potent drug candidate for it to exhibits its functions under physiological conditions, it is always important to analyze the electronic properties, environment dependent charge redistribution and dipolar interactions. The stock solutions (5 mM) of all complexes **4a**-**4b**, and **5a**-**5b** were prepared in methanol. The working concentration of all complexes was chosen as 5 μM in different solvents such as CH_2Cl_2 DMF, ethyl acetate and methanol of varying polarity. The electronic absorption or emission spectrum in water could not be recorded because of their poor solubility and the respective electronic spectrum are depicted in Figure S1 (see supporting information). The absorption spectra were recorded in all the above solvents in the range of 220 nm to 500 nm as shown in figure 2. The long wavelength absorption band of **4a** and **4b** compounds was centered ~280 nm and 330 nm and that of **5a** and **5b** compounds were centered ~280 nm. It can be observed from the absorption spectrum that for all the complexes the π - π^* transition band is in the range of ~250–360 nm and the charge transfer band in the range of ~360–500 nm under aqueous environment.

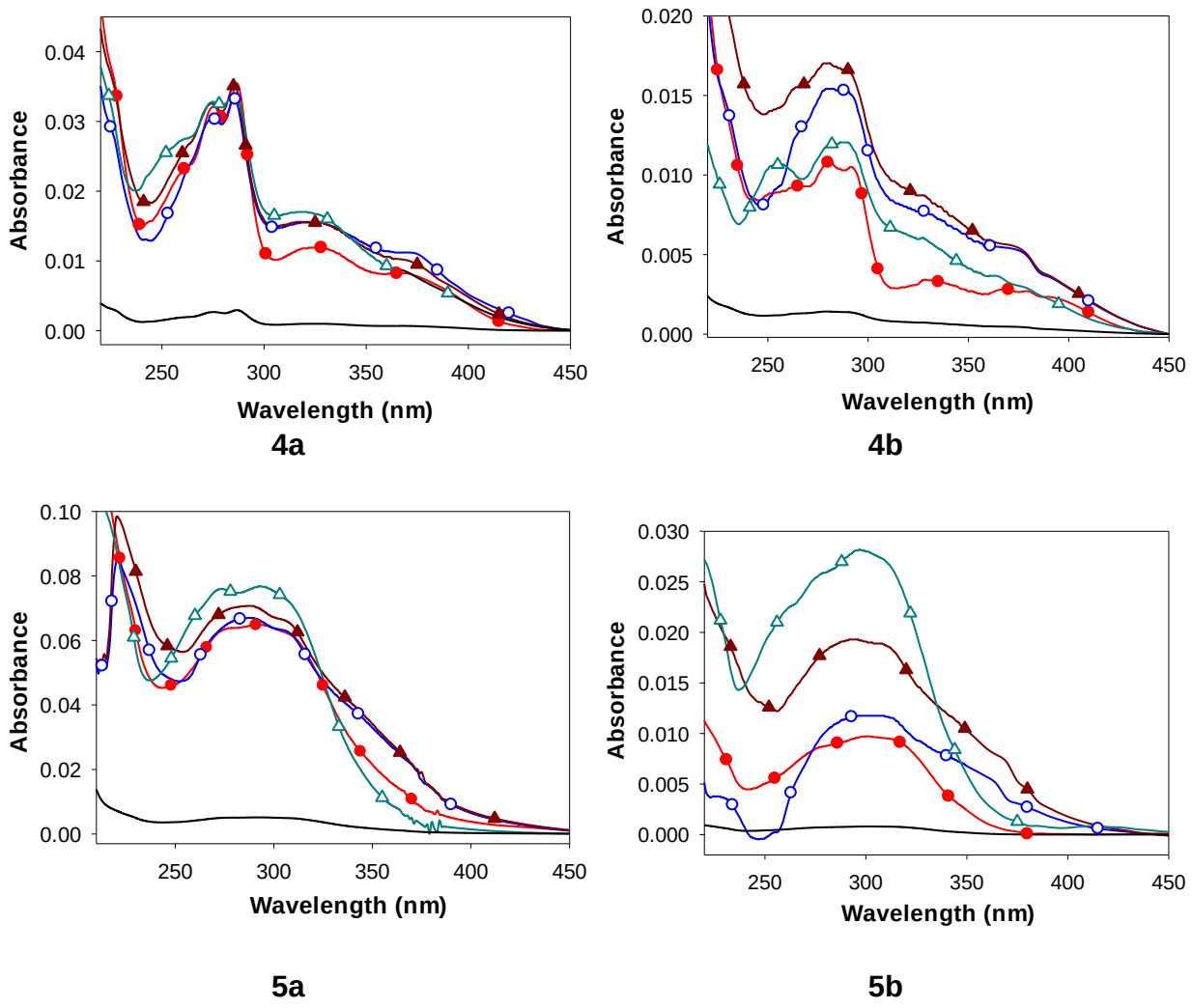

Figure 2. Absorption spectra depicting the observed solvatochromism of **4a-b** and **5a-b** in different solvents - ●, CH_2Cl_2; O, DMF; ▲, Ethylacetate and Δ, Methanol and ____ , Water.

The photophysical properties of the compounds in the excited state were investigated by steady state fluorescence emission spectra by exciting at 300 nm. The concentration of the samples was kept identical at 5 µM throughout the experiments. A red shift of 347, 597, 450 and 677 cm^{-1} respectively in complexes **4a**, **4b**, **5a**, and **5b**, when solvent polarity is increased from dichloromethane to dimethyl formamide. This could be due to the induced electronic charge redistribution upon excitation, thereby increasing the dipolar nature of the complexes. Moreover,

as the protic nature increases, the hydrogen bond forming capacity between the complex and the solvents increases that could stabilize them further. The luminescent properties as evaluated from the relative quantum yield were found to vary with the polarity of solvents. The values were found to increase with increasing polarity and protic nature of the solvents. This could be due to the fact that non polar interactions could induce non-radiative decay process as shown in figure 3. The variations observed in the quantum yield in all the solvents are shown in table 2.

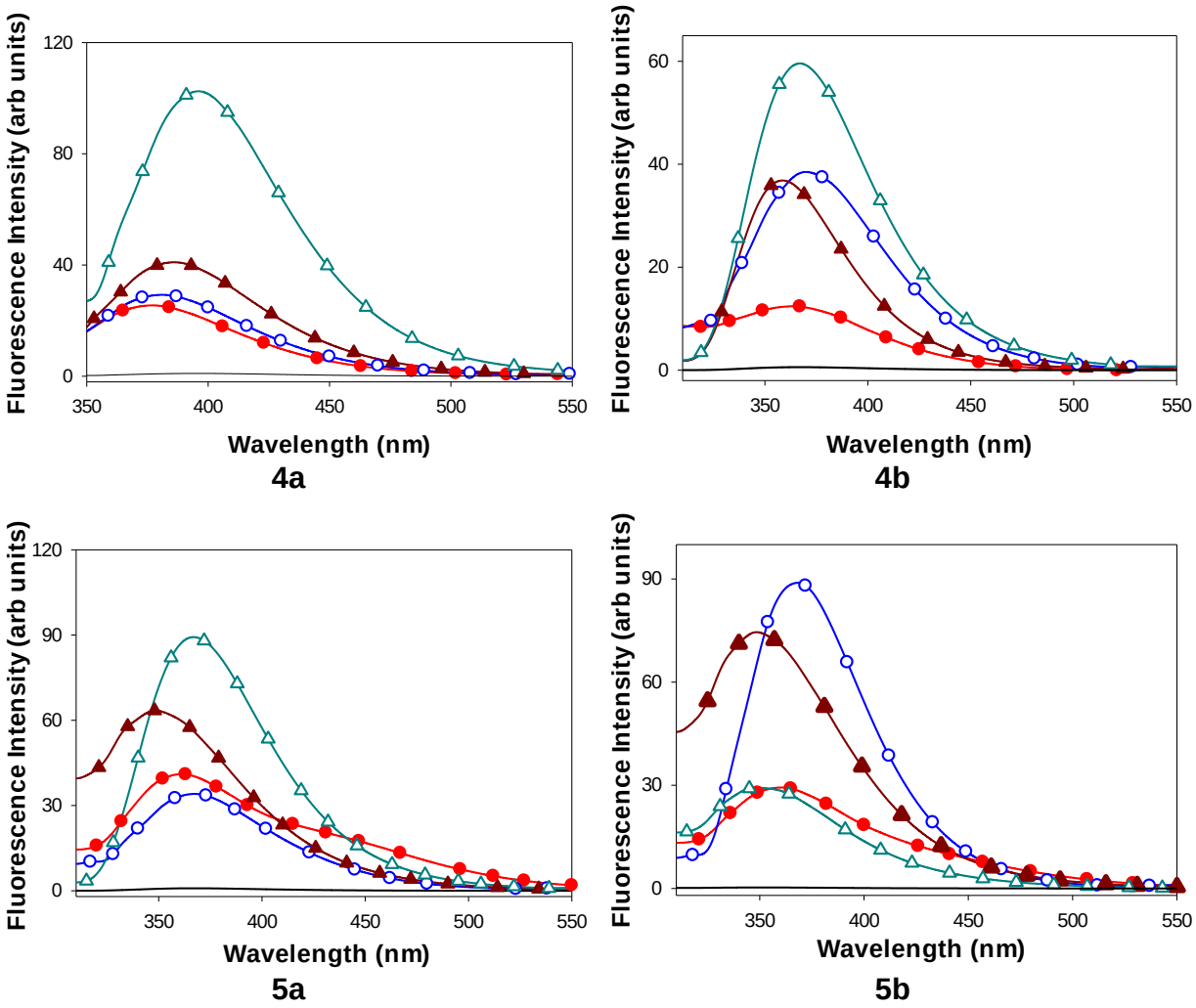

Figure 3. Fluorescence emission spectra depicting the observed solvatochromism of **4a – b** and **5a – b** in different solvents - ●, CH_2Cl_2; O, DMF; ▲, Ethylacetate and Δ, Methanol and ____ , Water.

Table 2. Absorption and fluorescence emission spectral characteristics of **4a-b** and **5a-b** complexes in different solvents.

Compound	Solvents	$\lambda_{max}^{ab}(log\ \varepsilon_{max})$	$\lambda_{max}^{fl}(\emptyset_{fl})$[a]
4a	Ethylacetate	263 (sh), **275** (3.81), **286** (3.85), **322** (3.49), 368 (sh)	386 (0.41)
	CH_2Cl_2	262 (sh), **275** (3.81), **286** (3.85), **324** (3.38), 368 (sh)	377 (0.09)
	DMF	263 (sh), **275** (3.78), **286** (3.82), **323** (3.49), 367 (sh)	382 (0.22)
	Methanol	262 (sh), **274** (3.82), **285** (3.83), **318** (3.53), 368 (sh)	396 (0.53)
	Water (pH 7.0)	273, 286 (-)	-
4b	Ethylacetate	265 (sh), **280** (3.53), 288 (sh), 321 (sh), 362 (sh)	359 (0.20)
	CH_2Cl_2	261 (sh), **280** (3.33), **292** (3.32), **330** (2.83), 375 (sh)	362 (0.01)
	DMF	266 (sh), **281** (3.49), 290 (sh), 320 (sh), 365 (sh)	370 (0.10)
	Methanol	**252** (3.32), 282 (sh), **288** (3.38), 320 (sh), 368 (sh)	367 (0.71)
	Water (pH 7.0)	282 (-)	-
5a	Ethylacetate	**285** (4.15), 339 (sh)	349 (0.15)
	CH_2Cl_2	276 (sh), **302** (4.10)	362 (0.14)
	DMF	**288** (4.13), 339 (sh)	368 (0.14)
	Methanol	259 (sh), **273** (4.18), **293** (4.19)	367 (0.16)
	Water (pH 7.0)	300 (-)	-
5b	Ethylacetate	**292** (3.59), 308 (sh), 339 (sh), 374 (sh)	349 (0.35)
	CH_2Cl_2	280 (sh), **302** (3.29)	360 (0.24)
	DMF	285 (sh), **302** (3.37), 340 (sh), 375 (sh)	369 (0.27)
	Methanol	266 (sh), 282 (sh), **296** (3.75)	351 (0.41)
	Water (pH 7.0)	-	-

[a] Quantum yield were determined using quinine sulphate as the standard ($\emptyset_{fl}$= 0.55 in water)

Subsequently, we turned our attention for the potential use of these complexes **4a-b**, and **5a-b** as therapeutic agents which can be assessed by their stability under ambient biological conditions of cells. Complexes **4a-b**, and **5a-b** were investigated for aqueous stability in water by UV-Vis spectroscopy for a period of 24 hours. Significant hypochromic shift was observed for **4a** and **4b** while **5a** and **5b** displayed slight hypochromic shift as shown in figure 4. As reported for other ruthenium complexes,[25] the observed shift could be due to the formation of aqua complex.

10.1002/cplu.202000516

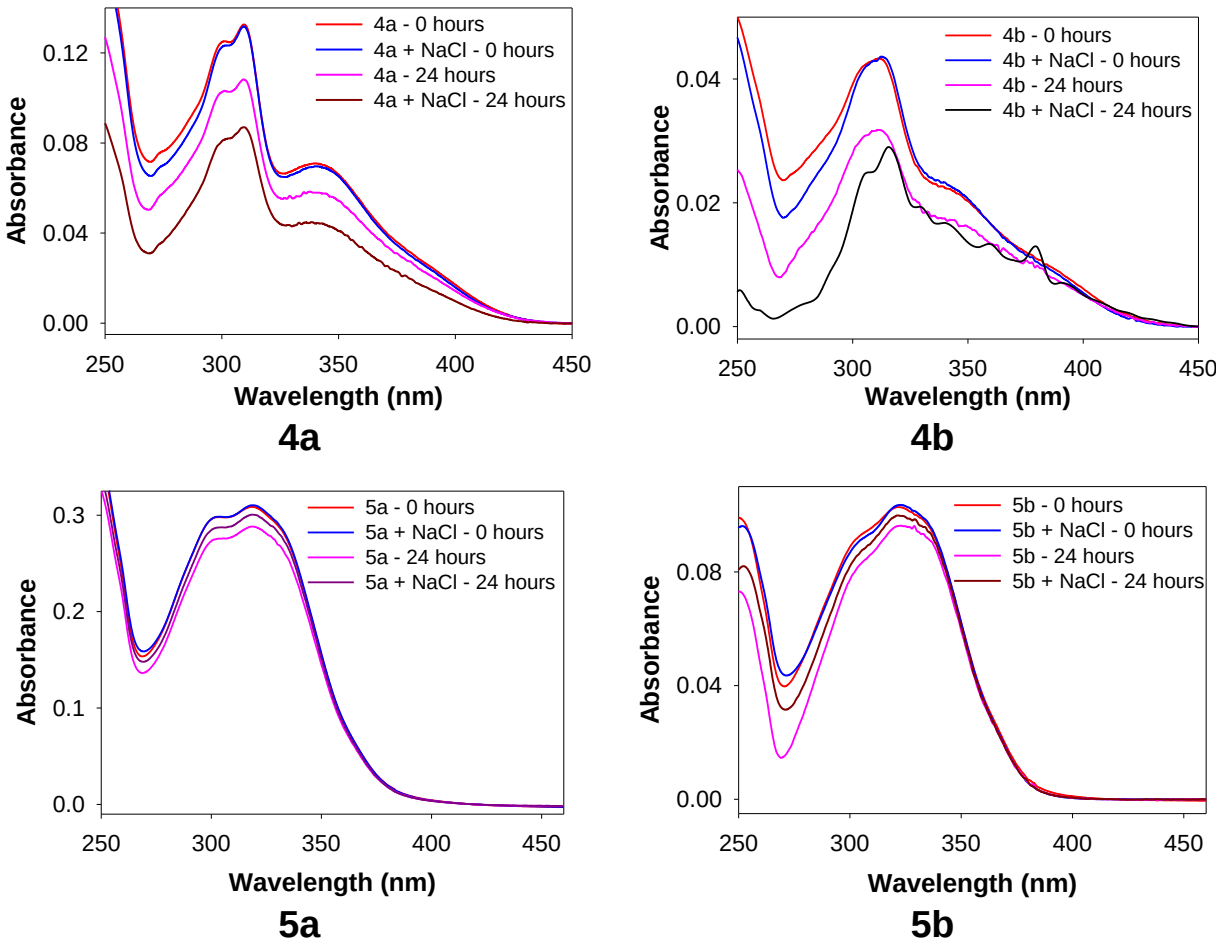

Figure 4: Stability of complexes **4a**, **4b**, **5a** and **5b** in presence and absence of 150 mM NaCl in 10 mM phosphate buffer, pH 7.2 and 5 % DMSO in a time interval of 0 and 24 hours.

The variation in the absorption spectra was also monitored in the presence of 1 mM GSH in 10 mM phosphate buffer, pH 7.2, under similar conditions. Significant changes were observed in the absorption spectra of **4a**, **4b**, **5a** and **5b** after an incubation period of 24 hours. Though the above results suggest that the complexes bind effectively with GSH, further investigations on its ability to interact with glutathione transferases will shed light on the above discussions.[26] The small hypochromic shift observed after 24 hours indicates that the complexes are stabilized by its ability to bind to GSH. The influence of NaCl on the above observed hypochromism was also investigated. In the absence of GSH, NaCl displayed negligible effect, whereas in the presence of

GSH, the hypochromism was suppressed significantly in the presence of 150 Mm NaCl for **5a** and **5b** specifically after a stipulated time period as mentioned in the figure 4 and figure 5. This indicates that under physiological conditions of high chloride ion concentrations the complexes **5a** and **5b** maintain better stability when compared with **4a** and **4b** in the presence of GSH as indicated in figure 5. Therefore under physiological conditions where the concentration of chloride ions is significantly low, these complexes can react with intracellular nucleophiles and hence can be considered as a scope for potent therapeutic agents.

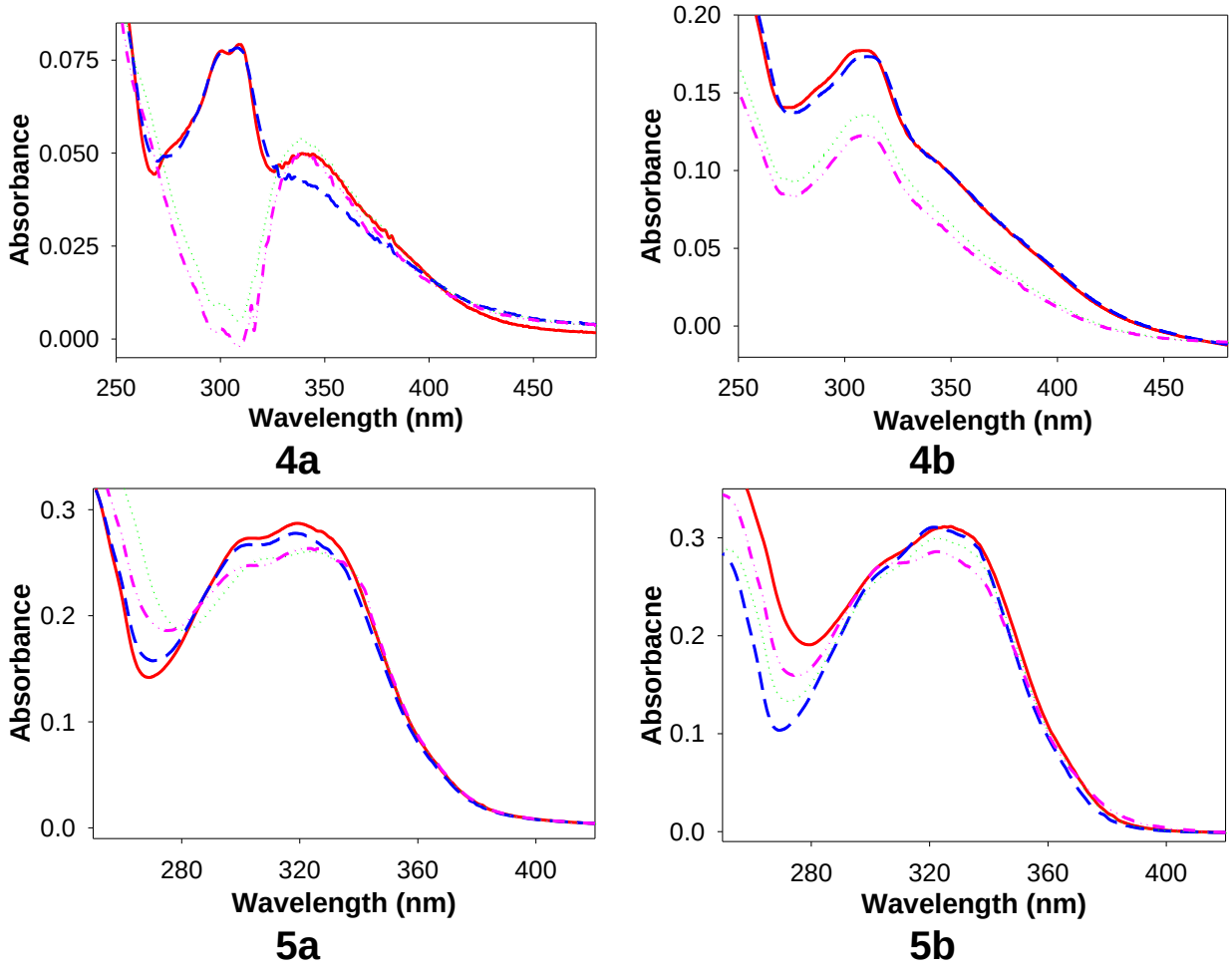

Figure 5: Stability of complexes **4a, 4b**, **5a** and **5b** in presence and absence of 150 mM NaCl in 10 mM phosphate buffer, pH 7.2 with 1 mM GSH and 5 % DMSO in a time interval of 0 and 24 hours. _____ 0 hrs, 0 mM NaCl; - - - - 0 hrs, 150 mM NaCl; ..... 24 hrs, 0 mM NaCl and ___.. 24 hrs, 150 mM NaCl

After synthesizing metal complexes **4a-b**, and **5a-b**, it is necessary to determine the cellular uptake behaviors of metal complexes which have been reported to be affected by many factors such as lipophilicity, molecular size, and the substituent group.[27] Lipophilicity is basically referred to as the partition coefficient of the compound in n-octanol/water (Po/w). The lipophilicity of metal complexes as calculated by the classical shake flask method[28] indicates the following trend: **5b** > **5a** > **4a** > **4b**. Among the iridium and ruthenium complexes, the iridium complexes **5b** and **5a** were moderately found to be more lipophilic. The possible reason for this observation could be the charge localization and the polarizability induced by the chelating ligands attached to the metal center. Increased polarizability could lead to increased hydrophilicity. Therefore, it could be inferred that ruthenium complexes **4a-b** are more polarized than iridium complexes **5a-b.** The in vitro cytotoxicity of synthesized metal complexes **4a-b**, **5a-b** and cisplatin was assessed by 3-(4,5-dimethylthiazol-2-yl)- 2,5-diphenyltetrazolium bromide (MTT) assay against different human cancer cell lines representing of human cervical cancer (HeLa), human breast adenocarcinoma (MCF-7), and human lung carcinoma (A549) respectively in a concentration-dependent manner and the values were compared when the ligands alone were used as control. The results of IC_{50} values are summarized in Table 3. Commercially available metallo drug cisplatin was used as a positive control. Among all the metal complexes evaluated, the compound **5b** showed good cytotoxicity against the tested cancer cell lines with the IC_{50} concentrations of 3.9 µM (HeLa), 4.5 µM (A549), 3.58 µM (MCF-7). Interestingly from Table 3,

it is also clear the compound **5b** showed stronger cytotoxicity at lower concentrations when compared to positive control cisplatin. Our earlier observations, as discussed above have shown that **5b** has higher stability in aqueous medium and higher lipophilicity compared to other complexes. Not limited to both or either of these could be responsible for the observed cytotoxicity. Moreover in order to evaluate the cytotoxicity of **5b** in the presence of light, phototoxicity experiment was carried out for **5b** against MCF-7 cell lines (see supporting information). The results revealed that the variation in the values of % cell viability was negligible when cytotoxicity was tested in light (IC_{50} = 3.55 μM) and dark (3.62 μM). Based on the above results, compound **5b** with an effective IC_{50} value of 3.5 μM was considered for further biological characterization using MCF-7 cell lines.

Table 3. Cytotoxicity of ligands and metal complexes **4a-b**, and **5a-b** expressed as IC_{50} values [μM] at 24 h.[a]

Compound	HeLa[b]	A549[c]	MCF-7[d]
3a	94.6 ± 0.24	>100	> 100
3b	33.4 ± 1.09	35.3 ± 0.60	32.9 ± 0.81
4a	> 100	54.6 ± 0.90	36.4 ± 1.05
4b	8.9 ± 0.43	21.9 ± 1.05	8.2 ± 0.42
5a	6.0 ± 0.79	10.7 ± 0.11	8.8 ± 0.50
5b	3.9 ± 0.36	4.5 ± 0.05	3.5 ± 0.05
Cisplatin	3.5 ± 0.48	7.0 ± 0.69	10.0 ± 1.00

[a] 50% inhibitory concentration values are an average of three individual experiments.
[b] Cervical cancer. [c] Lung cancer. [d] Breast cancer.

Further, to establish the cytotoxicity of iridium complex **5b** using cellular morphological changes, MCF-7 cell lines were incubated with 3.5 μM of compound **5b** for 24 h. The microscopic results indicated clear morphological alterations with the formation of rounded cells, with apoptotic morphology and decreased cell density due to cell death and the same is depicted in figure 6.

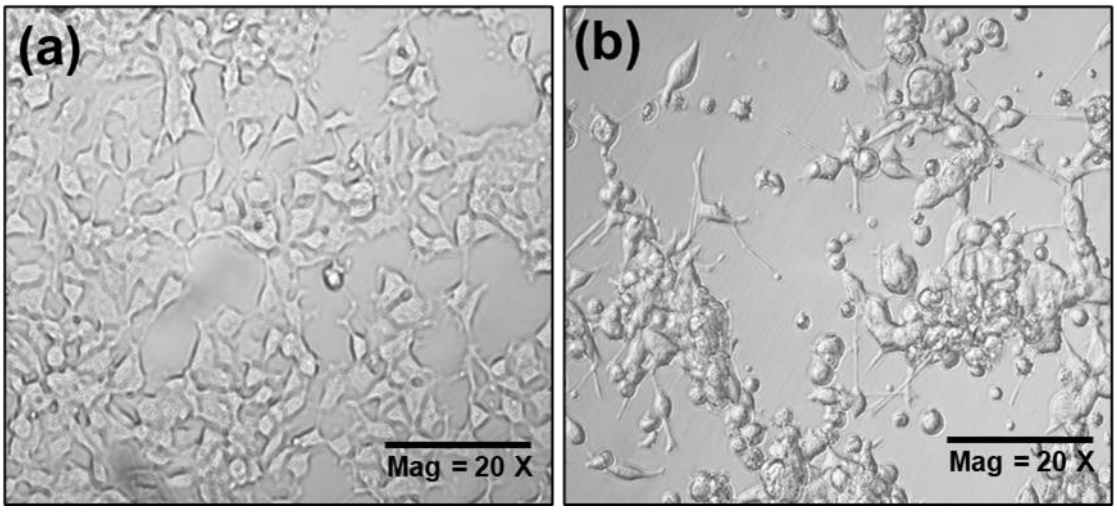

Figure 6. Iridium complex **5b** induced morphological changes in MCF-7 cell lines. (a) MCF-7 cells without treatment showing healthy morphology, (b) MCF-7 cells treated with complex **5b** at 3.5 µM showing altered morphology.

It is well established that cancer cells have the tendency for uncontrolled cell growth and proliferation, which results in the formation of colony like intensive growth under *in vitro* growth set up.[29] To establish the anti-proliferative effects of complex **5b**, we evaluated its interfering effect on colony formation in MCF-7 cells. The results showed that complex **5b** inhibited colony formation and significantly reduced the colony number and size in MCF-7 cells at IC_{50} value as shown in figure 7A(b) whereas control cells developed large number of colonies characterizing the proliferating cancerous cells as depicted in figure 7A(a).

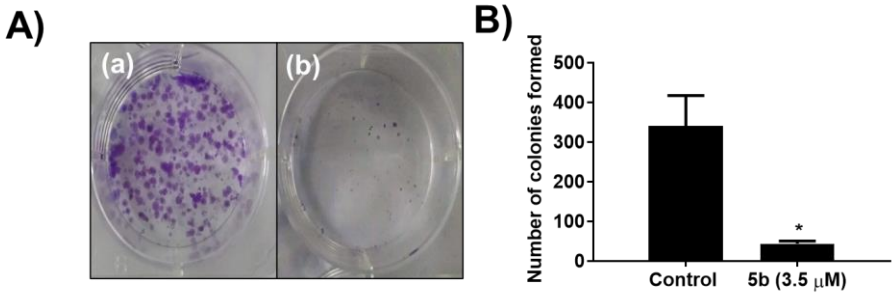

Figure 7. Iridium complex **5b** inhibited cell survival and colony formation in MCF-7 cell lines. A) The colony formation of (a) Control, (b) complex **5b** at 3.5 µM concentration, B) Histogram representing the corresponding quantification of colony numbers against concentration. All the images are representative of three independent experiments and data reported as mean ± SD; significant at the *$p < 0.005$.

Apoptosis, a programmed cell death is the major cell death principle which is a preferred mode for any cancer treatment options. Activation of executive enzymes, caspase-3 and -7, is a critical step during any apoptotic cell death process. The activated caspases will act on many downstream targets like nuclear, mitochondrial and cytoskeletal proteins which lead to ordered dismantling of cancer cells.[30] To check the effect of iridium complex **5b** on activation of caspase 3/7 in MCF-7 cell lines, we used an active caspase 3/7 reactive probe. The nucleic acid binding dye present in this reagent emits green fluorescence upon binding to cellular DNA, this process is inhibited in healthy cells through the inhibitory DEVD peptide. However, in the apoptotic cells, the activated caspase 3/7 cleave the inhibitory DEVD peptide and allow the fluorescent dye to bind DNA and emit green fluorescence. With our experiments, it is clearly evident that there is no green fluorescence observed in control cells as shown in figure 8a, whereas cells in figure 8b showed bright green fluorescence upon treatment with complex **5b** confirming the apoptotically activated caspase 3/7. Further, to observe the nuclear level morphological changes associated with apoptosis, like nuclear fragmentation, chromatin condensation were analyzed by DAPI staining in iridium complex **5b** treated MCF-7 cells. The DAPI is a nucleus specific fluorescent dye which efficiently binds to nucleic acid. In the apoptotic cells due to DNA fragmentation and chromatin condensation, the DAPI will emit bright blue fluorescence while non-apoptotic cells appear with regular blue color nucleus. Figure

8c demonstrated that control cells do not exhibit any apoptotic cell morphology and the nucleus was intact, whereas the figure 8d showed MCF-7 cells treated with 3.5 µM of iridium complex **5b** exhibited typical nuclear fragmentation and chromatin condensation, which are observed in majority of the cells and are represented by arrows. Phenotypically, cellular membrane blebbing is one of the distinct features of apoptosis. During apoptosis due to the changes in cellular cytoskeleton, the membrane bulges outwards as blebs, and these blebs later separates as apoptotic bodies. To check the formation of apoptotic blebs, and confirm the dying morphology, MCF-7 cells upon treatment with complex **5b** were observed under the scanning electron microscope. The figure 8f showed changes in the cell surface with the formation of apoptotic blebs after treatment with IC_{50} concentration of complex **5b** whereas in control cells no apoptotic morphology is seen and are with typical smooth surface as in figure 8e.

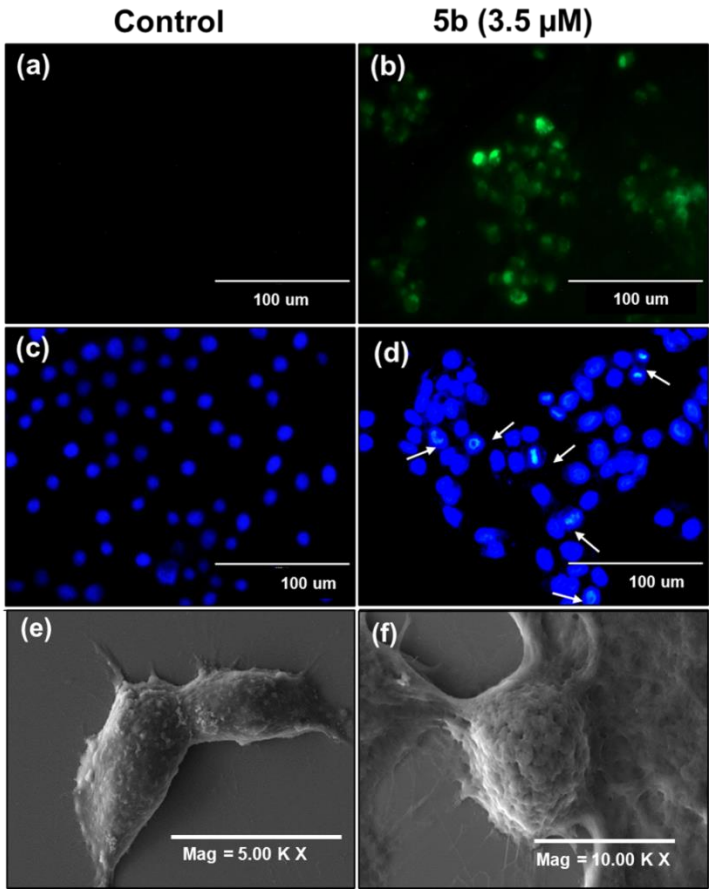

Figure 8. Iridium complex **5b** induced cellular apoptosis in MCF-7 cell lines: (a) & (b) Representing the caspase 3/7 activity, (c) & (d) Representing nuclear fragmentation by DAPI staining. The arrow marks indicate the fragmented nuclei induced by complex **5b**, (e) & (f) indicates the SEM images of MCF-7 cells showing apoptotic morphology. The images are representative of three independent experiments.

It is well known that the mortality risk of cancer patients increases mainly after spreading of cancer cells from the primary tumor site to secondary sites. Cellular migration and invasion are the crucial steps of metastasis, which play the important role of spreading cancer to distant organs.[31] To check the ability of iridium complex **5b** to inhibit *in vitro* cell migration, wound healing assay was performed. The results with MCF-7 cells demonstrated that the complex **5b**, when treated at its IC_{50} concentration, have significantly inhibited the migratory potential of MCF-7 cells as depicted in figure 9A(d) when compared to the control cells as shown in figure 9A(c).

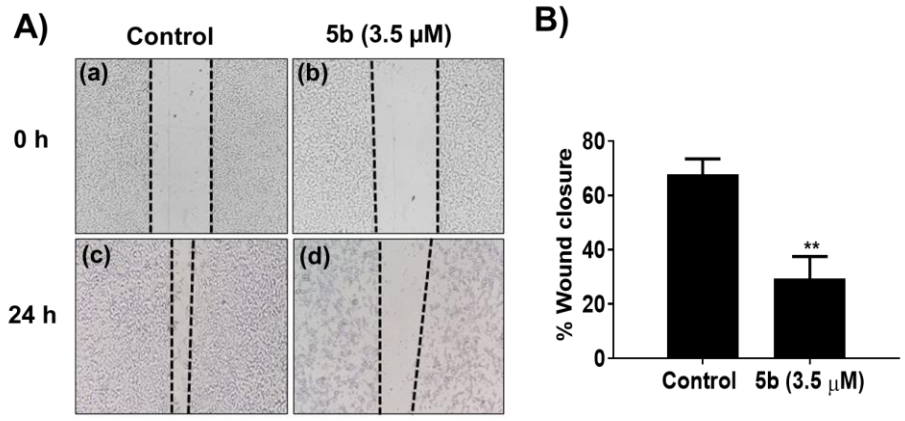

Figure 9. Iridium complex **5b** inhibited the migration of MCF-7 cell lines: A) Representative images of iridium complex **5b** inhibiting migration of MCF-7 cells. (a & b) 0^{th}-hour images of control and complex **5b** treatment groups. (c & d) 24^{th}-hour images of control and complex **5b** treatment groups. The lines represent the borders of the wound. B) graph representing the

 10.1002/cplu.202000516

percentage of wound closure at 24 h. Data represented is reported as mean ± SD with significance at the **p < 0.005 versus control.

It is always important to study the interaction of anticancer metallodrugs with biomolecules such as DNA, and proteins as they play a vital role in the biodistribution, mechanism of action, and enhanced toxicity.[32] Based on the above observations, herein we have chosen **5b** for further investigation on its interaction with calf thymus DNA (ct-DNA) and human serum albumin (HSA). The binding interaction of complexes with ct-DNA was investigated by following a competitive binding experiment in the presence of ethidium bromide and the mode of interaction was evaluated. Here eithidium bromide (EtBr) was not only used as a fluorescent probe but also as a competing agent to bind ct-DNA in the presence of complex **5b**. EtBr a planar cationic dye with phenanthridine ring is used as a fluorescence probe for native DNA. The intense fluorescence emission observed from EtBr in the presence of ct-DNA is due to strong interaction between adjacent DNA base pairs *via* intercalative binding. The remarkable decrease in fluorescence intensity of EtBr-ct-DNA with increasing concentration (0-100 μM) of the quencher **5b** was observed and is shown in Figure 10. The fluorescence intensity of the EtBr bound ct-DNA was quenched as its interaction with the **5b** replace the DNA bound to EtBr. The quenching constants of metal complexes were analyzed by following Stern-Volmer equation:

$$I_0 / I = 1 + K_{sv} [\mathrm{Q}] \qquad (1)$$

Here I_0 and I are the emission intensities in the absence and presence of quencher, respectively. K_{sv} is the linear Stern-Volmer quenching constant, and [Q] is the concentration of quencher in equation 1. The K_{sv} value was obtained from slope of I_0/ I vs. [Q]. The quenching plot depicts that the quenching of EtBr bound to ct-DNA by metal complexes are in good agreement with the Stern-Volmer equation. The quenching

constant values (K_{sv}) were found to be 13.2 μM^{-1}. The apparent binding constant (K_{app}) values for metal complexes were obtained from the following equation 2:

$$K_{EB}\,[EB] = K_{app}\,[complex] \quad \ldots\ldots\ldots\ldots\ldots\ldots\ldots\ldots (2)$$

Here $K_{EB} = 1.0 \times 10^7\ M^{-1}$, [EtBr] = 5 μM and [complex] is the complex concentration at 50 % reduction in the fluorescence intensity of EtBr. The quenching constant K_{app} value of **5b** was found to be 25.3 μM^{-1}. These results suggest that the complex **5b** bind with ct-DNA *via* intercalation mode and binding constant values are less while comparing with other classical intercalators.

Further to study the nature of interaction between HSA and the metal complexes, electronic spectrum of **5b** was recorded. HSA is the highly abundant blood serum proteins which serve as carrier for a wide range of ligands, drugs, and metal ions. The quenching effect was observed by titrating fixed amount of protein against varying concentration of complex **5b**. The decrease in the emission intensity of HSA with increasing amounts of **5b** indicates the type of interaction between protein and complex. As no shift in the absorption spectra is observed, it indicates a static quenching rather than dynamic quenching.

Mainly the presence of amino acids phenylalanine, tyrosine and tryptophan are the responsible for the observed fluorescence in HSA. Out of these three, tryptophan plays a major role in the intrinsic fluorescence of HSA. Fluorescence spectral titrations were carried out in the wave length range of 285-500 nm upon excitation at 280 nm. The effect of **5b** on fluorescence spectra of protein are shown in Figure 11. The increasing concentration of metal complexes (0 - 100 μM) shows a significant quenching of

fluorescence intensity at 345 nm, accompanied by a red shift. The observed shift could be due to the binding of metal complexes with one of the active sites of the protein.

In order to investigate the nature of the binding site, competitive titration was performed in the presence of **5b** along with warfarin (specifically binds to Site I) and dancyl glycine (specifically binds to Site II). The quenching of HSA fluorescence in the presence of warfarin indicates that **5b** binds to site I of HSA and results are shown in Figure 11.

The fluorescence quenching constant values are described by the Stern-Volmer equation as given above.

If small molecules bind independently to a set of equivalent sites on a macromolecule, the equilibrium between free and bound molecules is represented by the Scatchard equation:

$$\log [(I_0 - I)/ I] = \log K_b + n \log [Q]$$

Here K_b is the binding constant of the complex with HSA and n is the number of binding sites. Employing the plot of log $[(I_0 - I)/ I]$ *versus* log [Q], the number of binding sites (n) and the binding constant (K_b) values could be obtained. The quenching constant (K_q), binding constant (K_b) and number of binding sites (n) for the interaction of the complexes with HSA are 0.0377 x 10^6 M^{-1}, 0.046 x 10^6 M^{-1}, and 1 respectively. The results indicated that in complex **5b**, only one binding site is available for interaction with HSA.

10.1002/cplu.202000516

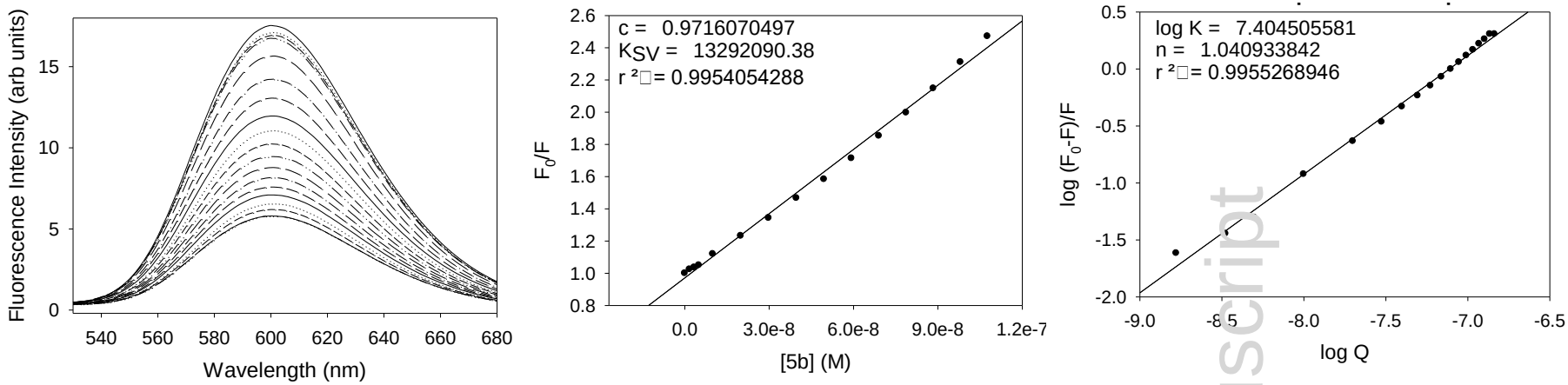

Figure 10. Fluorescence spectral titration showing the competitive quenching EtBr:DNA fluorescence by **5b**. (b) Stern-Volmer quenching plot for the titration of **5b** against EtBr:DNA complex (c) Scatchard plot

10.1002/cplu.202000516

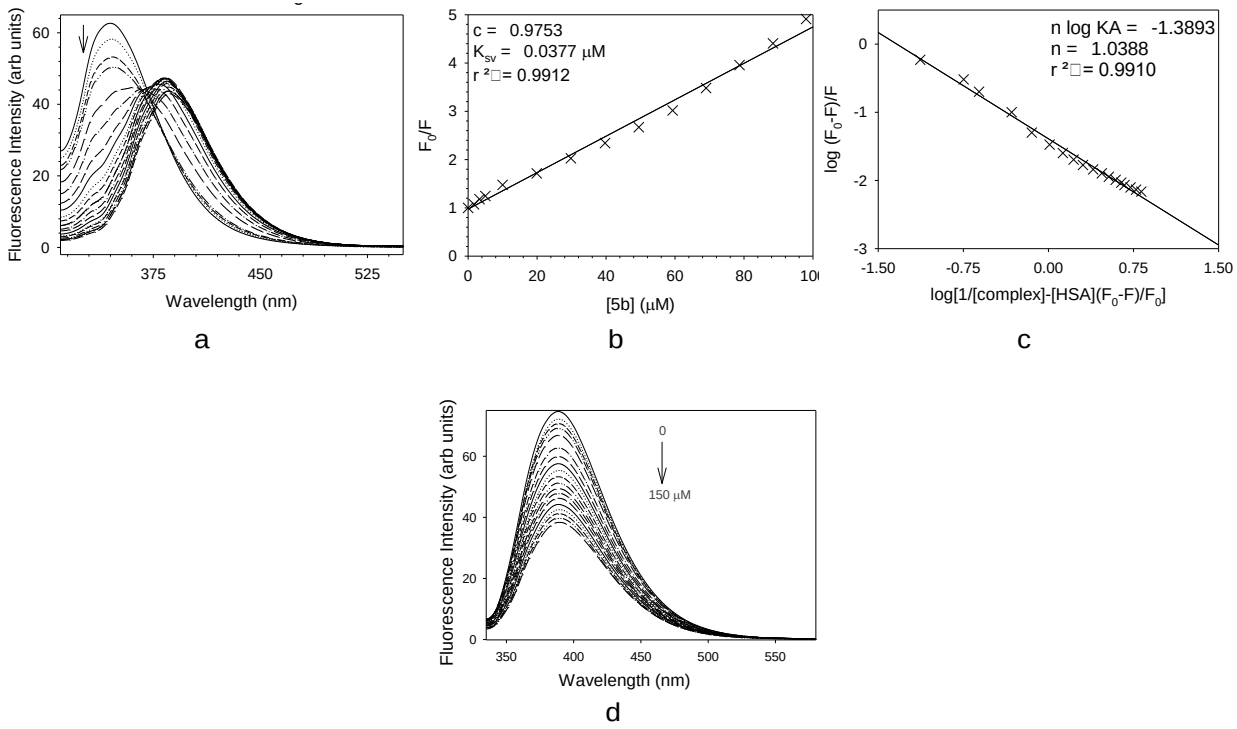

Figure 11. (a) The binding of **5b** with HSA as indicated by the fluorescence emission spectra. (b) The linear plot showing the Stern-volmer quenching effect (c) The scatchard plot for binding of **5b** with HSA. (d) Identification of binding site on HSA by the competition reaction of **5b** with warfarin specific for site I.

10.1002/cplu.202000516

The chemical nuclease activity of iridium complex **5b** was investigated using pBR322 plasmid DNA in 50 mM Tris-HCl buffer (pH = 7.2). Depending on the ability of the metal complexes to cleave the supercoiled DNA, the ratio of the three forms (supercoiled, nicked circular and open linear) will vary and can be identified from their electrophoretic mobility on agarose gel. Figure 12 depicts the results of agarose gel electrophoretic separations of various forms of pBR322 DNA in the presence of metal complex **5b**. As shown in Figure 12, in the presence of complexes, the supercoiled DNA is gradually converted into nicked circular and linear DNA depending on the cleaving ability. In addition, the oxidative cleavage of DNA in the presence of hydrogen peroxide is also studied by gel electrophoresis and is shown in Figure 12. It could be observed that in presence of hydrogen peroxide, the cleavage ability of **5b** was enhanced considerably as compared with other complexes.

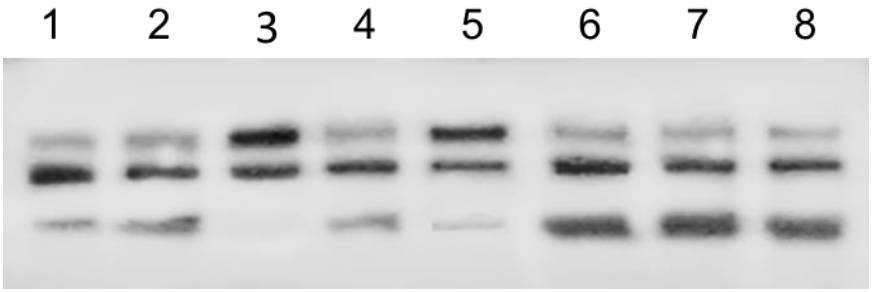

Figure 12. Agarose gel electrophoresis depicting the mobility of cleaved products of pBR322 by complex **5b** in the presence and absence of H_2O_2, DMSO (hydroxyl radical scavenger) and NaN_3 (singlet oxygen radical scavenger). Lanes 1: DNA; 2: DNA + **5b; 3:** DNA + **5b** + H_2O_2; 4: DNA + **5b** + H_2O_2 + DMSO; 5: DNA + **5b** + H_2O_2 + NaN_3; 6: DNA + H_2O_2; 7: DNA + H_2O_2 + DMSO; 8: DNA + H_2O_2 + NaN_3.

In order to investigate the cleavage mechanisms the reaction was carried out in the presence and absence of hydroxyl radical scavenger (DMSO) and singlet oxygen quencher (NaN_3). Inhibition

of DNA cleavage was observed in the present of NaN_3 indicating that $^1O_2$ is involved in the reaction. At the same time, when hydroxyl radical scavenger, DMSO is used the nuclease activity was significantly diminished indicating the involvement of the hydroxyl radical in the cleavage process. According to the results mentioned in figure 12, we propose the hypothesis that the complexes examined here may be capable of promoting DNA cleavage through an oxidative DNA damage pathway, in which the active oxygen species involved in the reaction are singlet oxygen, ($^1O_2$) and hydroxyl radical ($^{\cdot}OH$) at varying extents.

Conclusion

In conclusion, we have successfully synthesized a series of C-N cyclometalated 2*H*-indazole Ru(II) and Ir(III) complexes with substituents such as H, and isopropyl group in the R_4 position of the phenyl ring of 2*H*-indazole chelating ligand. The Ru(II) and Ir(III) complexes exhibit good anticancer activity against Hela, A549, and MCF-7 cancer cell lines. The new iridium complex **5b** with isopropyl substituent in the phenyl ring of 2*H*-indazole moiety showed good activity against MCF-7 cells and show apoptosis with increased caspase-3/7 activity. Further, the complex **5b** is capable of inhibiting cancer cell migration in MCF-7 cell line. Subsequently, the iridium complex **5b** bind to DNA *via* intercalation mode and bind to HSA at sites I.

Experimental Section

Chemistry

General Methods

Unless otherwise indicated all common reagents and solvents were used as obtained from commercial suppliers without further purification. ^1H NMR (400 MHz) and ^{13}C NMR (100

MHz) were recorded on a Bruker DRX400 spectrometer. Chemical shifts are reported in ppm relative to the internal solvent peak. Coupling constants, *J*, are given in Hz. Multiplicities of peaks are given as: d (doublet), m (multiplet), s (singlet), and t (triplet). Mass spectra were recorded on a Perkin Elmer Calrus 600 GC-MS spectrometer. High resolution mass spectra (HRMS) were recorded in ESI mode using Thermo Exactive LC-MS mass spectrometer. UV/vis spectroscopy was carried out on a UV-2550, Shimadzu Corporation, and Kyoto, Japan. The fluorescence spectra were recorded on Hitachi F-7000 FL spectrophotometer. Solvents were dried by the usual methods. $[(\eta^6\text{-}p\text{-cymene})RuCl_2]_2$, $[(\eta^5\text{-}C_5Me_5)IrCl_2]_2$, sodium salt of calf thymus DNA, ethidium bromide (EB), human serum albumin (HSA) were obtained from Sigma-Aldrich (Bangalore, India); pBR322 plasmid DNA used in the studies were obtained from Sigma-Aldrich (Bangalore, India). The synthesis of metal complexes **4a-b**, and **5a-b** was carried out from previously reported literature method with a slight modification.[12f]

General Procedure for the Synthesis of substituted 2*H*-indazole Ru(II) complexes 4a-b.

In a round bottomed flask equipped with magnetic bar under nitrogen atmosphere, 2-phenyl-2*H*-indazole (1 mmol) **3a** was dissolved in a freshly distilled dichloromethane solution (5mL)**.** Sodium acetate (1.2 mmol) was added in to the flask at room temperature with constant stirring followed by the addition of $[(\eta^6\text{-}p\text{-cymene})RuCl_2]_2$ (0.5 mmol). The reaction mixture was stirred at room temperature for 20h and the progress of reaction was monitored by TLC. After completion of the complex formation, diethyl ether (10 mL) was added in the mixture. Reaction mixture was stirred for 10 min to precipitate out the product. The crystalline product was filtered through a fritted funnel and dried well. The yellow colored ruthenium complex **4a** was obtained in good yield with 72% yield. R_f = 0.25 (40%EtOAc/*n*-hexane); ^{1}H NMR (400 MHz, $CDCl_3$) δ 8.43 (s, 1H), 8.23 (d, J = 7.2 Hz, 1H), 7.98 (d, J = 8.8 Hz, 1H), 7.66 (d, J = 8.4 Hz,1H), 7.47-

7.43 (m, 2H), 7.20-7.16 (m, 2H), 7.05 (dd, *J* = 6.8, 1.6 Hz, 1H), 5.93 (d, *J* = 5.8 Hz, 1H), 5.74 (d, *J* = 5.8 Hz, 1H), 5.41 (d, *J* = 5.8 Hz, 1H), 5.17 (d, *J* = 5.8 Hz, 1H), 2.28-2.23 (m,1H), 2.11 (s, 3H), 0.88 (d, *J* = 6.90 Hz, 3H), 0.72 (d, *J* = 6.90 Hz, 3H); ^{13}C NMR (100MHz, $CDCl_3$) δ 148.5, 141.1, 140.5, 128.0, 127.2, 123.4, 122.8, 121.5, 118.4, 115.9, 113.1, 102.3, 99.1, 89.5, 89.3, 82.4, 81.0, 30.7, 22.5, 21.7, 18.9; MS (ESI, MS) 429 $(M\text{-}Cl)^+$; HRMS (ESI, m/z) calcd for $C_{23}H_{23}N_2Ru$: m/z 429.0905; Found 429.0903.

Compound **4b** was synthesized using similar procedure for synthesis of compound **4a.** Yield: 75%; pale yellow solid; R_f = 0.27 (40%EtOAc/n-hexane); ^{1}H NMR (400 MHz, $CDCl_3$) δ 8.34 (s, 1H), 8.01 (s, 1H), 7.90 (d, *J* = 8.8 Hz, 1H), 7.62 (d, *J* = 8.4 Hz, 1H), 7.38 (d, *J* = 6.8 Hz, 1H), 7.36-7.32 (m, 1H), 7.14 -7.10 (m, 1H), 6.89 (d, *J* = 8.0 Hz, 1H), 5.83 (d, *J* = 5.8 Hz, 1H), 5.69 (d, *J* = 5.8 Hz, 1H), 5.29 (d, *J* = 5.8 Hz, 1H), 5.09 (d, *J* = 5.8 Hz, 1H), 2.97-2.90 (m,1H), 2.26-2.19 (m, 1H), 2.03 (s, 3H), 1.29-1.26 (m, 6H), 0.85 (d, *J* = 6.90 Hz, 3H), 0.68 (d, *J* = 6.90 Hz, 3H); ^{13}C NMR (100MHz, $CDCl_3$) δ 147.4, 146. 138.2, 137.7, 127.4, 126.8, 121.6, 120.3, 116.9, 114.9, 111.7, 101.1, 98.4, 88.7, 88.0, 80.9, 79.9, 33.2, 29.7, 28.6, 23.6, 22.9, 21.5, 20.6; MS (ESI, MS) 471 $(M\text{-}Cl)^+$; HRMS (ESI, m/z) calcd for $C_{26}H_{29}N_2Ru$: m/z 471.1374; Found 471.1341.

In a round bottomed flask equipped with magnetic bar under nitrogen atmosphere, 2-phenyl-2*H*-indazole (1 mmol) **3a** was dissolved in a freshly distilled dichloromethane solution (5mL)**.** Sodium acetate (1.2 mmol) was added in to the flask at room temperature with constant stirring followed by the addition of $[(\eta^5\text{-}C_5Me_5)IrCl_2]_2$ (0.5 mmol). The reaction mixture was stirred at room temperature for 20 h and the progress of reaction was monitored by TLC. After completion of the complex formation, dichloromethane was distilled under reduced pressure and diethyl ether (10 mL) was added in the mixture. Reaction mixture was stirred for 10 min to precipitate out the product. The crystalline product was filtered through a fritted funnel and dried well. The

orange colored iridium complex **5a** was obtained in good yield with 82% yield. R_f = 0.26 (40% EtOAc/*n*-hexane); ^{1}H NMR (400 MHz, $CDCl_3$) δ 8.37 (s, 1H), 7.89 (d, *J* = 7.2 Hz, 1H), 7.72-7.66 (m, 2H), 7.52 (d, *J* = 8.0 Hz, 1H), 7.36 (t, *J* = 7.6 Hz, 1H), 7.20-7.16 (m, 2H), 7.07 (dd, *J* = 8.0, 1.2 Hz, 1H), 1.76 (s, 15H); ^{13}C NMR (100MHz, $CDCl_3$) δ 147.7, 146.9, 136.9, 128.4, 128.3, 122.9, 122.7, 121.6, 119.1, 115.2, 112.4, 88.5, 9.6; MS (ESI, MS) 521 $(M\text{-}Cl)^+$; HRMS (ESI, m/z) calcd for $C_{23}H_{25}ClIrN_2$: m/z 557.1336; Found 557.1349.

Compound **5b** was synthesized using similar procedure for synthesis of compound **5a.** Yield: 85%; Pale yellow solid; R_f = 0.34 (40%EtOAc/*n*-hexane); ^{1}H NMR (400 MHz, $CDCl_3$) δ 8.69 (s, 1H), 7.72 (d, *J* = 7.2 Hz, 1H), 7.51 (d, *J* = 8.4 Hz, 2H), 7.29-7.27 (m, 2H), 7.19-7.15 (m, 1H), 7.05 (dd, *J* = 7.6, 1.2 Hz, 1H), 3.02-2.95 (m, 1H), 1.4 (s, 15H), 1.30 (d, *J* = 7.2 Hz, 6H); ^{13}C NMR (100MHz, $CDCl_3$) δ 148.4, 147.5, 146.7, 140.3, 135.1, 128.1, 122.5, 121.5, 118.6, 115.1, 112.1, 88.4, 34.1, 24.7, 23.7, 9.6; MS (ESI, MS) 564 $(M\text{-}Cl)^+$; HRMS (ESI, m/z) calcd for $C_{26}H_{31}IrN_2$: m/z 564.2116; Found 564.2114.

Biology

Chemicals and reagents

Tissue culture plates, Dulbecco's modified eagle medium (DMEM), fetal bovine serum (FBS), trypsin-EDTA, and all the other cell culture products were purchased from Himedia (Mumbai, India). 3-(4,5-Dimethylthiazol-2-yl)-2,5-diphenyltetrazolium bromide (MTT) was purchased from Himedia (Mumbai,India). Cisplatin was purchased from Sigma Aldrich (Bangalore, India), Cell Event Caspase-3/7 Green Ready Probes Reagent was purchased from Thermo Fisher scientific (Bangalore, India).

Cell lines and cell culture conditions

MCF-7 (human breast adenocarcinoma cells), HeLa (human cervical cancer cells), A549 (human lung carcinoma) cell lines were obtained from National center for cell sciences (NCCS) Pune,

India. All the cells were maintained in DMEM supplemented with 10% FBS, 100 U/mL penicillin, 100 µg/ml streptomycin and 2.5 µg/ml Amphotericin B. Cell were maintained in a humidified incubator at 37 °C with 5% CO_2 atmosphere.

Cell Viability Assay

MTT (3-(4,5-Dimethylthiazol-2-yl)-2,5-diphenyltetrazolium bromide) assay was performed to check the cytotoxicity of metal complexes on three different cancer cell lines MCF-7, A549, and HeLa. Briefly, 5000 cell/well were seeded in 96 well plates and incubated for 24 h, and then treated with different concentrations of complexes **4a-b**, and **5a-b** for 24h. The spent medium was removed and cells were incubated with 25 µl of MTT solution (5mg/ml in 1XPBS) for 4 h. At the end of incubation purple-colored formazan formed was dissolved by adding 100 µl of DMSO. The absorbance was measured at 490 nm by using ELISA plate reader (BioTek-ELx800) and percentage viability calculated by plotting percentage viability against the concentration. The final concentration of DMSO does not exceed more than 0.25% in all the experiments.

Colony formation assay

Colony formation assay was performed to analyze the anti-proliferative effect of compound **5b** on MCF-7 cells. Cells were seeded at a density of 1000 cells/well in 6 well tissue culture plates and left for attachment at 37 °C. Then cells were treated with 3.5 µM of **5b** and control cells were left without treatment. Cells were allowed to form colonies for 14 days, spent media was removed and cells were washed thrice with 1X PBS. Colonies were fixed with 4% paraformaldehyde for 10 min and stained with 0.5% crystal violet for 20 min. The number of colonies was counted both in the treated and untreated samples.

Cell morphology by inverted microscope

To check the changes in cellular morphology in the presence and absence of **5b** on the MCF-7 cell line, cells were treated and examined under an inverted microscope. Briefly, 1×10^5 cells were seeded in 6-well tissue culture plates and incubated for 24 h. cells were treated or not treated(control) with 3.5 µM of IR-3 for 24 h after reaching 70-80% confluency. Images were taken under an inverted microscope (MAGNUS 10J617).

Caspase 3/7 activity assay

Caspase 3/7 activity in **5b** treated MCF-7 cells was detected by using caspase 3/7 green ready probe reagent (Invitrogen) according to the manufacturer protocol. Briefly, 1×10^5 cells were seeded on to the coverslips in 6-well tissue culture plates and incubated for 24 h. After reaching 70-80% confluency cells were treated or not treated(control) with 3.5 µM of **5b** for 24 h. Into each well of the 6-well plate, two drops of caspase probe were directly added and incubated at 37 °C for 30 min. After the incubation, the coverslips were removed from the wells and mounted on the clean glass slides. The activation of caspase 3/7 in Ir3 treated cells was observed under a fluorescence microscope (EVOS FL cell imaging system) and images were captured.

DAPI (4′,6-diamidino-2-phenylindole) staining

To check the apoptotic nuclear fragmentation induced by **5b** on MCF-7 cells, DAPI staining was performed. Briefly, 1×10^5 cells were seeded on to the coverslips placed in 6-well plates and incubated for 24 h. The control cells were maintained without the addition of the metal complex and treatment group was added with 3.5 µM of **5b** for 24 h. then the coverslips were rinsed thrice with 1X PBS, fixed with 4% paraformaldehyde for 10 min, stained with DAPI and incubated in dark for 10 min. The cells were checked for apoptotic nuclear fragmentation under a fluorescence microscope (EVOS FL cell imaging system).

Scanning electron microscopy (SEM) analysis

SEM analysis was performed to check the effect of **5b** on inducing apoptotic morphology in MCF-7 cells. Briefly, 1×10^5 cells were seeded on to the glass coverslips placed in six-well plates and left for the attachment. After the cells reached 70-80% confluency the cells were incubated with 3.5 µM of **5b** and control cells were left untreated for 24 h. cells were then aspirated with 1X PBS for thrice and fixed with 2.5% glutaraldehyde for 2h at room temperature. Then the cells were dehydrated by washing with 30, 40, 60, 70, 80, 95 and 100% ethanol, and kept for drying at 37 °C for 48 h. then the cells were coated with gold examined under SEM (Zeiss Evo 18 microscope).

Wound healing assay

To check the effect of **5b** on cell migration of MCF-7 cells, wound healing assay has been performed**.** The MCF-7 cells at a cell density of 1×10^5 cells/well were plated in a 6-well plate and incubated for 24 h. Later the spent media was removed and a wound was made by using a sterile 200 µl pipette tip and cells were treated with 3.5 µM of **5b** and control cells were left untreated for 24 h. The length of the wound was measured at 0^{th} h and 24 h of the treatment and images were taken under an inverted microscope ((MAGNUS 10J617).

Statistical analysis

The values obtained in the experiments are expressed as mean ± Standard deviation (SD. For two group comparision a two-sided unpaired student t-test (using GraphPad Prisim 6 software) was used. All the experiments were done in triplicates and the representative data are shown. A P-value of $p<0.05$ is considered to be significant.

Supporting Information Summary

^1H, ^{13}C NMRs and IR and Mass spectral data for new compounds; Procedure for the lipophilicity

test; Absorption and fluorescence spectra of complexes in 5% DMSO in water; Dose dependent cytotoxicity study for complex **5b** in MCF-7 cells under light and dark conditions.

Acknowledgements

The authors thank the Chancellor and Vice Chancellor of VIT University for providing opportunity to carry out this study. Further the authors RNR, RLP, VM, MMB, and KC wish to thank the management of this university for providing seed money as research grant. Kaushik Chanda thanks CSIR-Govt. of India for funding through Grant no 01(2913)/17/EMR-II. Thanks are also to Central instrumentation facility VIT University for recording the spectra.

Keywords: Antitumor activity • Cyclometalated complexes • DNA • Iridium • Ruthenium

References:

[1] G. Rubner, K. Bensdorf, A. Wellner, B. Kircher, S. Bergemann, I. Ott, R. Gust, *J. Med. Chem.* **2010**, *53*, 6889-6898.

[2] A. Torreggiani, C. Chatgilialoglu, C. Ferreri, M. Melchiorre, S. Atrian, M. Capdevila, *J. Proteomics* **2013**, *92*, 204-215.

[3] C. E. Randolph, D. J. Foreman, S. K. Betancourt, S. J. Blanksby, S. A. McLuckey, *Anal. Chem*. **2018**, *90*, 12861-12869.

[4] J. T. Brewster, H. Zafar, H. D. Root, G. D. Thiabaud, J. L. Sessler, *Inorg. Chem*. **2020**, *59*, 32-47.

[5] M. Faizan, N. Muhammad, K. U. K. Niazi, Y. Hu, Y. Wang, Y. Wu, H. Sun, R. Liu, W. Dong, W. Zhang, Z. Gao, *Materials* **2019**, *12*, 1643.

[6] S. A. Andres, K. Bajaj, N. S. Vishnosky, M. A. Peterson, M. S. Mashuta, R. M. Buchanan, P. J. Bates, C. A. Grapperhaus, *Inorg. Chem*. **2020**, *59*, 4924-4935.

[7] a) C. N. Banti, A. D. Giannoulis, N. Kourkoumelis, A. M. Owczarzak, M. Kubicki, S. K. Hadjikakou, *Dalton Trans*. **2014,** *43*, 6848-6863. b) K. D. Mjos, C. Orvig, *Chem. Rev*. **2014**, *114*, 4540-4563.

[8] L. Isaacs, *Acc. Chem. Res*. **2014**, *47*, 2052-2062.

[9] X. Wang, X. Wang, S. Jin, N. Muhammad, Z. Guo, *Chem. Rev*. **2019**, *119*, 1138-1192.

[10] N. Cutillas, G. S. Yellol, C. Haro, C. Vincente, V. Rodríguez, J. Ruiz, *Coord. Chem. Rev*. **2013**, *257*, 2784-2797.

[11] L. R. Kelland, *Nat. Rev. Cancer* **2007**, *7*, 573-584.

[12] a) J. M. Hearn, I. Romero-Canelón, B. Qamar, Z. Liu, I. Hands-Portman, P. J. Sadler, *ACS Chem. Biol*. **2013**, *8*, 1335-1343. b) W. Liu, R. Gust, *Chem. Soc. Rev*. **2013**, *42*, 755-773; c) G. Gasser, I. Ott, N. Metzler-Nolte, *J. Med. Chem.* **2011**, *54***,** 3-25. d) I. Canelón, R. L. Salassa, P. J. Sadler, *J. Med. Chem*. **2013**, *56***,** 1291-1300. e) W. X. Ni, W. L. Man, S. M. Yiu, M. Ho, M. T. –W. Cheung, C. C. Ko, C. M. Che, Y. W. Lam, T. C. Lau, *Chem. Sci.* **2012**, *3*, 1582-1588. f) J. Yellol, S. A. Pérez, A. Buceta, G. Yellol, A. Donaire, P. Szumlas, P. J. Bednarski, G. Makhloufi, C. Janiak, A. Espinosa, J. Ruiz, *J. Med. Chem.* **2015**, *58*, 7310-7327.

[13] a) J. M. Rademaker-Lakhai, D. van den Bongard, D. Pluim, J. H. Beijnen, J. H. Schellens, *Clin. Cancer Res*. **2004**, *10*, 3717-3727. b) M. Sojka, M. Fojtu, J. Fialova, M. Masarik, M. Necas, R. Marek, *Inorg. Org*. **2019**, *58*, 10861-10870.

[14] a) P. Nowak-Sliwinska, C. M. Clavel, E. Paunescu, M. T. te Winkel, A. W. Griffioen, P. J. Dyson, *Mol. Pharmaceutics* **2015**, *12*, 3089-3096. b) R. W. Y. Sun, M. F. Ng, E. L. Wong, J. Zhang, S. S. Chui, L. Shek, T. C. Lau, C. M. Che, *Dalton Trans.* **2009**, *42***,** 10712-10716. c) V.

Vidimar, C. Licona, R. Ceron-Camacho, E. Guerin, P. Coliat, A. Venkatasamy, M. Ali, D. Guenot, R. Le Lagadec, A. C. Jung, J. N. Freund, M. Pfeffer, G. Mellitzer, G. Sava, C. Gaiddon, *Cancer Lett.* **2019**, *440-441*, 145-155.

[15] a) S. K. Tripathy, U. De, N. Dehury, P. Laha, M. K. Panda, H. S. Kim, S. Patra, S. *Dalton Trans*. **2016**, *45*, 15122-15136. b) A. Colombo, M. Fontani, C. Dragonetti, D. Roberto, J. A. G. Williams, R. Scotto di Perrotolo, F. Casagrande, S. Barozzi, S. Polo, *Chem. Eur. J.* **2019**, *25*, 7948-7952. c) G. Ghosh, K. L. Colón, A. Fuller, T. Sainuddin, E. Bradner, J. McCain, S. M. A. Monro, H. Yin, M. W. Hetu, C. G. Cameron, S. A. McFarland, *Inorg. Chem*. **2018**, *57*, 7694-7712. d) C. Licona, J.-B. Delhorme, G. Riegel, V. Vidimar, R. Cerón-Camacho, B. Boff, A. Venkatasamy, C. Tomasetto, P. D. F. Celestino Gomes, D. Rognan, J.-N. Freund, R. Le Lagadec, M. Pfeffer, I. Gross, G. Mellitzer, C. Gaiddon, *Inorg. Chem. Front*. **2020**, *7*, 678-688.

[16] S. Qian, J. Cao, Y. Yan, M. Sun, H. Zhu, Y. Hu, Q. He, B. Yang, *Mol. Cell. Biochem*. **2010**, *345*, 13-19.

[17] W. Han, J. C. Pelletier, C. N. Hodge, *Bioorg. Med. Chem. Lett*. **1998**, *8*, 3615-3620.

[18] X. Li, S. Chu, V. A. Feher, M. Khalili, Z. Nie, S. Margosiak, V. Nikulin, J. Levin, K. G. Sparankle, M. E. Fedder, R. Almassy, K. Appelt, K. M. Yager, *J. Med. Chem*. **2003**, *46*, 5663-5673.

[19] M. D. Angelis, F. Stossi, K. A. Carlson, B. S. Katzenellenbogen, J. A. Katzenellenbogen, *J. Med. Chem*. **2005**, *48*, 1132-1144.

[20] a) C. K. Chung, P. G. Bulger, B. Kosjek, K. M. Belyk, N. Rivera, M. E. Scott, G. R. Hunphery, J. Limanto, D. C. Bachert, K. M. Emerson, *Org. Process Res. Dev*. **2014**, *18*, 215-227. b) Y. Jia, J. Zhang, J. Feng, F. Xu, H. Pan, W. Xu, *Chem. Biol. Drug Des*. **2014**, *83***,** 306-

316. c) S. Tomassi, J. Lategahn, J. Engel, M. Keul, H. L. Tumbrink, J. Ketzer, T. Mühlenberg, M. Baumann, C. Schultz-Fademrecht, S. Bauer, D. Rauh, *J. Med. Chem*. **2017**, *60*, 2361-2372.

[21] J. Catalán, J.; J. C. del Valle, R. M. laramunt, G. Boyer, J. Aynez, J. Gómez, P. Jiménez, F. Tomás, J. Elguero, *J. Phys. Chem*. **1994**, *98*, 10606-10612.

[22] a) Y. Liu, R. Hammitt, D. A. Lutterman, L. E. Joyce, R. P. Thummel, C. Turro, *Inorg. Chem*. **2009**, *48*, 375-385. b) C. Mari, V. Pierroz, S. Ferrari, G. Gasser, *Chem. Sci*. **2015**, *6*, 2660-2686. c) F. Schmitt, P. Govindaswamy, G. Suss-Fink, W. H. Ang, P. J. Dyson, L. Juillerat-Jeanneret, B. Therrien, *J. Med. Chem*. **2008**, *51*, 1811-1816. d) S. C. Boca, M. Four, A. Bonne, B. van der Sanden, S. Astilean, P. L. Baldeck, G. Lemercier, *Chem. Commun*. **2009**, 4590-4592. e) F. E. Poynton, S. A. Bright, S. Blasco, D. C. Williams, J. M. Kelly, T. Gunnlaugsson, *Chem. Soc. Rev*. **2017**, *46*, 7706 - 7756,

[23] a) H. Huang, S. Banerjee, P. J. Sadler, *ChemBioChem* **2018**, *19*, 1574-1589. b) T. Huang, Q. Yu, S. Liu, K. Y. Zhang, W. Huang, Q. Zhao, *ChemBioChem* **2019**, *20***,** 576-86. c) E. M. Boreham, L. Jones, A. N. Swinburne, M. Blanchard-Desce, V. Hugues, C. Terryn, F. Miomandre, G. Lemercier, L. S. Natrajan, *Dalton Trans*. **2015**, *44*, 16127-16135.

[24] a) R. N. Rao, B. Maiti, K. Chanda, *ACS Comb. Sci*. **2017**, *19*, 199-228. b) R. N. Rao, M. M. Balamurali, B. Maiti, R. Thakuria, K. Chanda, K. *ACS Comb. Sci*. **2018**, *20*, 164-171. c) R. L. Panchagam, V. Manickam, K. Chanda, *ChemMedChem* **2019**, *14*, 262-272. d) R. D. Padmaja, M. M. Balamurali, K. Chanda, *J. Org. Chem*. **2019**, *84*, 11382-11390. e) R. N. Rao, K. Chanda, *Bioorg. Chem*, **2020**, *99*, 103801.

[25] Y. K. Yan, M. Melchart, A. Habtemariam, P. J. Sadler, *Chem. Commun*. **2005**, 4764-4776.

[26] A. De Luca, L. J. Parker, W. H. Ang, C. Rodolfo, V. Gabbarini, C. Nancy N. C. Hancock, F. Palone, A. P. Mazzetti, L. Menin, J. Morton, M. W. Parker, M. L. Bello, P. J. Dyson, *Proc. Nat. Acad. Sci.* **2019**, *116*, 13943-13951.

[27] F. X. Wang, M. H. Chen, Y. N. Lin, H. Zhang, C. P. Tan, L. –N. Ji, Z. W. Mao, *ACS Appl. Mater. Interfaces* **2017**, ***9***, 42471−42481.

[28] a) E. Rutkowska, K. Pajak, K. Jozwiak, *Acta Pol. Pharm*. **2013**, *70,* 3-18. b) M. C. Wenlock, T. Potter, P. Barton, R. P. Austin. *J. Biomol. Screen*. **2011**, ***16***, 348-355.

[29] A. Munshi M. Hobbs R. E. Meyn (2005) Clonogenic Cell Survival Assay. In: Blumenthal R.D. (eds) Chemosensitivity. Methods in Molecular Medicine™, vol 110. Humana Press.

[30] Y. Shi, *Protein Sci.* **2004**, *13*, 1979-1987.

[31] a) C. Wittekind, M. Neid, *Oncology* **2005**, *69*, 14-16; b) A. Mantovani, *Nature* **2009**, *457*, 36–37.

[32] O. Domotor, C. G. Hartinger, A. K. Bytzek, T. Kiss, B. K. Keppler, E. A. Enyedy, *J. Biol. Inorg. Chem.* **2013**, *18*, 9-17.

10.1002/cplu.202000516

Table of Contents

A series of novel C-N cyclometalated 2*H*-indazole Ru(II) and Ir(III) complexes were synthesized and evaluated for their anticancer activity against Hela, A549, and MCF-7 cell lines. The iridium complex with isopropyl substituent in the phenyl ring of 2*H*-indazole moiety exhibited apoptosis with increased caspase-3/7 activity and inhibited cell migration in MCF-7 cell line. Further these complexes were not active for photodynamic therapy and the observed anticancer activity could be induced by their bio-macromolecular interactions as revealed by protein and DNA binding abilities.